



Cite this: *Soft Matter*, 2019, 15, 6127

## Effects of poly(ethylene glycol) on the wetting behavior and director configuration of lyotropic chromonic liquid crystals confined in cylinders†

Hyesong Lee,<sup>a</sup> Vijaya Sunkara,<sup>b</sup> Yoon-Kyoung Cho <sup>bc</sup> and Joonwoo Jeong <sup>\*ab</sup>

We investigate the effects of poly(ethylene glycol) (PEG) doping on nematic lyotropic chromonic liquid crystals (LCLCs) confined in a cylindrical cavity. First, PEG added to Sunset Yellow (SSY) renders confining glass surfaces nemato-phobic by adsorption. We also confirm that the grafting of PEG to bare glass surfaces changes them from nemato-philic to nemato-phobic. This change in the wetting behavior affects how nematic director configurations form and relax. Additionally, we observe that PEG-doped nematic SSY retains the double-twist director configuration as in the PEG-free case. However, the PEG-doped nematic SSY is accompanied by unprecedented domain-wall-like defects and heterogeneity in the director configuration. We propose multiple hypotheses on how PEG changes the director configuration, including the formation of meta-stable director configurations.

Received 7th May 2019,  
Accepted 1st July 2019

DOI: 10.1039/c9sm00927b

[rsc.li/soft-matter-journal](http://rsc.li/soft-matter-journal)

Lyotropic chromonic liquid crystals (LCLCs) have become a field of active investigation because of their ubiquity, bio-compatibility, and unusual liquid-crystalline elastic properties.<sup>1–3</sup> The LCLC phases are ubiquitously found in dyes, drugs, and biomolecules such as short nucleic acids. In the LCLC phases, the molecules of a planar shape form face-to-face aggregates *via* non-covalent interactions in water. The elongated aggregates align to acquire orientational ordering and exhibit the nematic phase and columnar phase according to the concentration and temperature. A centrosymmetric unit vector called the director represents the local average direction of the aggregates. The nematic LCLC phases formed by the aggregates are known for their unusual elastic properties, *i.e.*, a large elastic anisotropy.<sup>4,5</sup> Namely, their twist elastic modulus  $K_2$  is much smaller than the splay and bend moduli, which often results in spontaneous chiral symmetry breaking of confined LCLCs despite the absence of intrinsic chirality in the LCLCs.<sup>6–10</sup> Additionally, they have an unprecedentedly large saddle-splay elastic modulus,  $K_{24}$ , which is supported by another observation of chiral symmetry breaking, *e.g.*, a double-twist (DT) director configuration in cylinders.<sup>11–13</sup>

Another prominent characteristic of LCLCs is their aqueous and non-surface-active nature. This allows various interactions between LC mesogens and their water-soluble or -dispersible additives and objects. It is different from the case of typical lyotropic LC phases formed by amphiphilic molecules, *e.g.*, phospholipids and detergents. While the amphiphilic molecules may adsorb on additives to screen them out or disrupt the structures of additives, *e.g.*, dis-assembly of cell membranes, chromonic aggregates often allow dissolved additives and dispersed objects to function normally. Thus, there have been a series of studies focusing on interactions between LCLCs and water-soluble additives as well as swimming bacteria in LCLCs.<sup>2,14,15</sup> First of all, as in thermotropic chiral nematic phases, water-soluble chiral dopants that induce chiral nematic LCLCs have been identified with the measurement of their helical twisting powers.<sup>16–27</sup> Additionally, the effects of salts on the aggregate behaviors, phase diagram, and LC elasticity have been actively investigated.<sup>28–46</sup> In a similar context, the effect of different functional groups on the phase diagram has been studied,<sup>39</sup> and even the phase diagram of the mixture of two different LCLCs is characterized.<sup>47</sup>

In addition to small molecules, macromolecules such as polymers have been investigated as additives to LCLCs. They are mostly exploited as crowding agents in LCLCs<sup>6,10,41,48</sup> and as the encapsulation layers to make water-solvated LCLC droplets.<sup>49</sup> The examples include polyelectrolytes and neutral poly(ethylene oxide), which affects the phase diagram considerably.<sup>48,50</sup> It is noteworthy that most of the studies with additives have been focused on their effects on LCLC phase behavior; only a few studies investigate how salts and surfactants affect the elastic moduli and the quality of LC alignment, respectively.<sup>51–54</sup>

<sup>a</sup> Department of Physics, School of Natural Science, Ulsan National Institute of Science and Technology (UNIST), Ulsan 44919, Republic of Korea.  
E-mail: [jjeong@unist.ac.kr](mailto:jjeong@unist.ac.kr)

<sup>b</sup> Center for Soft and Living Matter, Institute for Basic Science, Ulsan 44919, Republic of Korea

<sup>c</sup> Department of Biomedical Engineering, School of Life Science, Ulsan National Institute of Science and Technology (UNIST), Ulsan 44919, Republic of Korea

† Electronic supplementary information (ESI) available. See DOI: 10.1039/c9sm00927b

Here we report on the effects of neutral polymer doping on the wetting behavior and director configurations of confined LCLCs, beyond the phase behaviors of doped LCLCs. Specifically, we observe Sunset Yellow (SSY) confined in glass capillary tubes with and without poly(ethylene glycol) (PEG). First, the added PEG changes the wetting behavior of the nematic-isotropic coexistence phase under confinement. With the addition of PEG, the confining glass surfaces change from nemato-philic to nemato-phobic surfaces. To investigate the role of PEG, we conduct a systematic investigation by varying the concentration and molecular weight of the PEG added to bulk and grafting PEG to the confining surfaces. Additionally, we report PEG-induced changes in the director configuration: the emergence of a domain-wall-like defect, which is energetically unfavorable in the neat case, and a heterogeneity in the director configuration. This observation may indicate significant changes in LCLCs' properties and the surface anchoring. We propose multiple scenarios regarding PEG's effects on the director configuration.

## Materials and methods

### Sample preparation

Sunset Yellow (SSY, Sigma-Aldrich) of >90% purity is further purified following a published precipitation method.<sup>55</sup> The purified SSY powder is dissolved in deionized water (18.2 MΩ cm). We also dissolve poly(ethylene glycol) (PEG, Sigma-Aldrich) in deionized water to attain a PEG solution. We use PEGs of various average molecular weights ranging from 400 to 35 000. Finally, we mix two solutions of SSY and PEG to make the PEG-doped nematic SSY solution of desired final concentrations, *e.g.*, 30.0% (wt/wt) SSY and PEG with the concentration ranging from 10<sup>-3</sup> to 0.5% (wt/wt).

We put the PEG-doped nematic SSY solution into glass capillaries of cylindrical and square cross-sections by capillary force. The capillaries are purchased from Vitrocom and used as received. The capillaries after filling are fixed onto a glass slide by gluing their ends using an epoxy adhesive; this also helps to minimize the evaporation of water from the sample. To facilitate the optical imaging of the curved specimen, *i.e.*, the cylinders, we place a coverslip on top of the fixed capillaries and fill the volume between the slide and coverslip with a refractive index matching oil ( $n = 1.474$  at a wavelength of 589.3 nm, Cargile). After the assembly of the sample cell, every sample is heated to a fully isotropic phase and cooled to a nematic phase at 21.5 °C at the rate of 2–4 °C min<sup>-1</sup> on a temperature stage (Linkam T95-PE120) attached to the microscope. Then, we let them relax for over 4 hours before the observation. Unless we specify the temperature, all the observations and measurements are made at room temperature, *i.e.*, 21.5 °C.

For the grafting of PEG to glass surfaces, *i.e.*, pegylation, we take advantage of PEG with a silane functional group. For a short PEG chain, we use *N*-(triethoxysilylpropyl)-*o*-polyethylene oxide urethane (molecular weight = 400–500, Gelest). For long PEG chains, we use mPEG-silane with molecular weights of 2000, 5000, and 20 000 (Laysan Bio). First, we clean glass surfaces (Duran) by dipping

them into a 10% NaOH solution for 3 minutes at 70 °C. After thorough rinsing with copious amounts of deionized water, the glasses are dried and incubated with 10 mM mPEG-silane solution in toluene for 2 hours. The glass slides are rinsed with toluene once, dried at room temperature, and baked in an oven at 110 °C for 40 minutes. Finally, we clean the glasses with sonication in ethanol and dry them thoroughly. Contact angle analysis and X-ray photoelectron spectroscopy confirm the successful grafting of PEG to the glass surfaces (see Fig. S1 in the ESI†).

### Polarized optical microscopy and characterization of director configuration by Jones calculus

All optical microscopy images are taken using an Olympus BX-53P equipped with a color CCD (Infinity3-6UR, Lumenera) under quasi-monochromatic illumination (center wavelength = 660 nm, FWHM = 25 nm; LED4D067, Thorlabs). For polarized optical microscopy (POM), a polarizer and an analyzer can be rotated freely to observe the sample. For phase retardation experiments, we place a full-wave plate (optical path difference = 550 nm) in front of the analyzer. To characterize the director configuration, we measure the intensities of the transmitted quasi-monochromatic light through the center of a capillary as a function of angle between the pass axes of the polarizer and the analyzer. The center of the capillary is designated to be a wide rectangle spanning 10 percent of the capillary diameter. Initially, both polarizer and analyzer are set parallel to the cylindrical axis. Then we measure the transmitted intensities while rotating only the analyzer by 5 degrees counterclockwise.

## Results and discussion

### Effects of PEG on the wetting behavior of the nematic-isotropic coexistence phase

We first identify the phases of PEG-doped SSY in cylindrical capillaries. The effects of PEG on the phase diagram of SSY are well characterized; PEG doping drives the nematic phase into the nematic-isotropic coexistence phase because PEG works as a crowding agent.<sup>48</sup> Here, we find that the concentration and molecular weight of PEG are critical in this crowding effect. For instance, when the molecular weight of the added PEG is as small as 400, the doping concentration up to 0.1% (wt/wt) does not seem to affect the phase and director configuration of nematic SSY. On the other hand, the more we add PEG of high molecular weight, *e.g.*, 35 000, the more the isotropic regions of the nematic-isotropic coexistence phase appear. We experimentally estimate that the critical concentration of 35k PEG for the appearance of the coexistence phase in 30.0% (wt/wt) SSY at room temperature is approximately 0.01% (wt/wt). Fig. 1(a) and (b) show the typical POM texture of a fully nematic phase of neat SSY in a cylindrical capillary, *i.e.*, the double-twist (DT) director configuration. By contrast, as shown in Fig. 1(c) and (d), based on the doping concentration tiny isotropic droplets could be dispersed in the nematic phase, or isotropic regions may separate nematic domains.

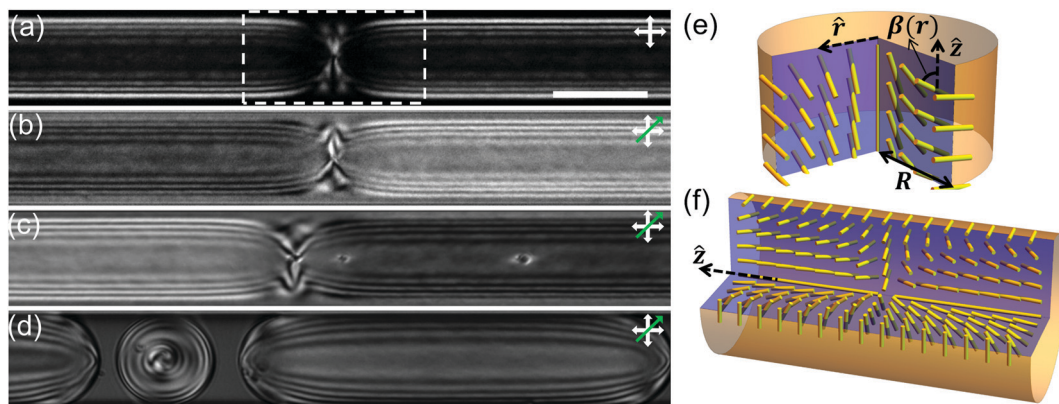


**Fig. 1** Double-twist (DT) director configuration of nematic SSY confined in cylindrical cavities and the schematic diagrams of its director configuration and topological defect. (a and b) POM images of the DT director configuration of 30.0% (wt/wt) nematic SSY between crossed polarizers (a) without and (b) with a full-wave plate (550 nm retardation) under quasi-monochromatic illumination at a wavelength of 660 nm. White double arrows represent the pass axes of the linear polarizers and a green single-headed arrow indicates the slow axis of the full-wave plate. Scale bar: 50  $\mu\text{m}$ . The stripe patterns result from the modulation of the phase retardation determined by continuously changing the optical path length of the cylindrical cavity and nematic directors along the optical path in the DT configuration. The singular pattern surrounded by a dashed box corresponds to a point defect between the left and right domains of different handednesses. The difference in the handedness is manifested in (b) by the insertion of the full-wave plate. (c and d) POM images of the DT configuration of the nematic SSY doped with 35k PEG with concentrations of (c) 0.01% (wt/wt) and (d) 0.5% (wt/wt). The tiny droplets in the right domain of (c) and the stripe-pattern-free regions in (d) are the PEG-induced isotropic phase in the nematic–isotropic coexistence phase. (e) The schematic diagram of the DT configuration. The yellow rods represent the nematic directors. The angle between the director and the capillary axis  $\hat{z}$  is  $\beta$  as a function of radius  $r$ ; in the DT configuration, the director does not have a radial component. (f) The director configuration of the point defect highlighted by a dashed box in (a) according to Davidson *et al.*<sup>11</sup>

PEG doping affects how the nematic phases grow and finds their equilibrium director configuration. In the neat SSY without PEG, as fully isotropic SSY enters the region of nematic–isotropic coexistence phase by temperature decrease, the nematic phase grows from the confining walls of the capillaries as shown in Fig. 2(a)–(c).<sup>13</sup> Namely, in the coexistence phase, a cylindrical shell of the nematic phase wraps around the isotropic core. As the temperature decreases further, the shell gets thicker, and the core gets slenderer to break up eventually because of the Plateau–Rayleigh instability. The whole process is shown in Movie S1 in the ESI.† After this breakup, the nematic domains are separated by isotropic droplets and keep growing before SSY reaches the fully nematic phase while they find the equilibrium director configuration, the DT configuration, *via* relaxation. In the end, the isotropic droplets generated from the break-up disappear to make the sample fully nematic. We emphasize that bare glass surfaces are nemato-philic in the case of neat SSY because the nematic phase grows from the glass surface.

To our surprise, a minuscule amount of PEG added to SSY completely changes the wetting behavior of the nematic–isotropic coexistence phase of SSY. As shown in Fig. 2(d)–(f), with the addition of 0.01% (wt/wt) 35k PEG into the nematic SSY, spherical nematic droplets of twisted bipolar configuration<sup>7</sup> nucleate in the bulk instead of the growth of nematic films on the glass confining walls when the sample enters the coexistence phase from the isotropic phase. We confirm that sodium chloride or a chiral dopant, *i.e.*, brucine sulfate heptahydrate,<sup>9</sup> added to SSY does not induce this wetting reversal; when PEG is added, the nemato-phobic glass confining wall favors the isotropic phase over the nematic phase. As the temperature decreases further to room temperature, the nematic droplets grow and merge to

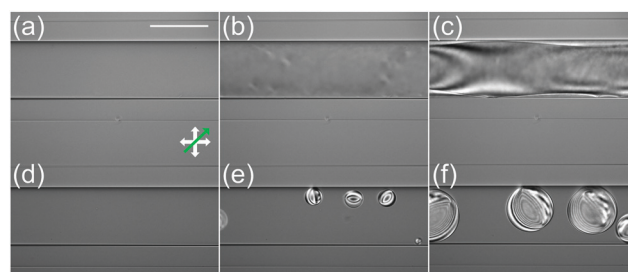


**Fig. 2** POM images of the isotropic-to-nematic phase transition of SSY confined in cylindrical cavities 100  $\mu\text{m}$  in diameter. Scale bar: 100  $\mu\text{m}$ . (a–c) Neat 30.0% (wt/wt) SSY with no PEG. (d–f) 30.0% (wt/wt) SSY with 0.01% (wt/wt) 35k PEG. Initially, in (a and d), the samples are fully isotropic at  $56 \pm 1$   $^{\circ}\text{C}$ . Then, we decrease the temperature at the rate of  $1 \text{ K min}^{-1}$ . In (b and e), the isotropic-to-nematic phase transition occurs as the temperature becomes  $54 \pm 1$   $^{\circ}\text{C}$ . Upon further decrease in temperature, *i.e.*, around  $50 \pm 1$   $^{\circ}\text{C}$ , the nematic regions expand as shown in (c and f). Note that two samples with and without PEG doping are on the same slide glass at the same temperature; namely, (b and e) are at the same temperature. The brightness pattern starts to appear in (b) because the birefringent nematic film emerges on the wall of the cylinder as SSY enters the nematic–isotropic coexistence phase. The cylindrical nematic shell becomes thicker in (c). In contrast, with the addition of PEG, nematic droplets nucleate in the bulk instead of the nematic film on the cylinder wall.

form the DT configuration eventually (see Fig. 1(c) and (d)). With this low concentration, PEG doping does not seem to affect the isotropic–nematic transition temperature by  $\pm 1$   $^{\circ}\text{C}$ .

Further investigations suggest that the surface adsorption of PEG onto the confining wall causes the change in the wetting behavior. Longer PEGs at higher concentrations adsorb more to the surfaces.<sup>56</sup> This adsorption behavior of PEG is consistent with our observation. First, we use PEGs of different molecular

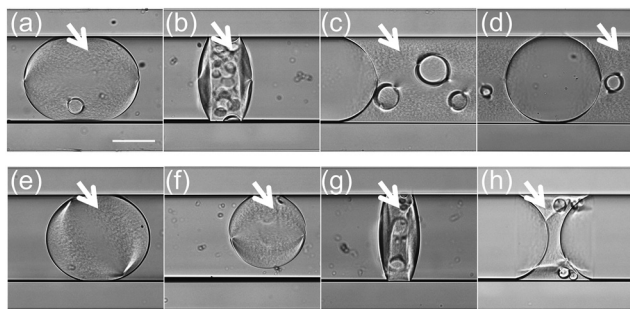


**Fig. 3** Effects of molecular weight and concentration of PEG on the wetting behavior of the nematic–isotropic coexistence phase of 26.0% (wt/wt) SSY at room temperature. The sample is confined in a 200  $\mu\text{m}$  diameter capillary. Short white arrows indicate nematic regions. (a–c) SSY with 0.01% (wt/wt) PEG with an average molecular weight of 35k, 1k, and 400, respectively. (d) Neat SSY with no PEG. (e–h) SSY with 0.1, 0.01, 0.001, and 0.0001% (wt/wt) of 8k PEG, respectively. Scale bar: 100  $\mu\text{m}$ .

weights ranging from 400 to 35 000 as dopants to dope SSY and observe the wetting of the nematic phase on the glass in the nematic–isotropic coexistence phase. To observe the coexistence phase at room temperature, we utilize samples of a relatively low concentration of SSY, *i.e.*, 26.0% (wt/wt). As shown in Fig. 3(a)–(d), we observe that PEGs of lower molecular weights have less effect on the wetting behavior. Specifically, the contact angle of the nematic domain on the glass wall, as shown in Fig. 3(a), with 0.01% (wt/wt) 35k PEG is close to 180 degrees, while the nematic domain with PEG 400 (Fig. 3(c)) exhibits complete wetting on the glass as in the case of neat SSY (Fig. 3(d)). Short white arrows point out the nematic regions in Fig. 3. For instance, a nematic droplet is located in the center of Fig. 3(a), and the nematic regions surround the isotropic droplet in Fig. 3(d). Secondly, we also vary the doping concentration of PEG from  $1.0 \times 10^{-3}$  to 0.1% (wt/wt) and find that the glass becomes nemato-phobic as we increase the doping concentration. Note that we refrain from quantifying the contact angles because there could be optical distortion at the interface because of the curved LCLC–glass interface. Although the glass capillaries are immersed in the index-matching oil to minimize refraction, the mismatch of refractive indices between the glass and SSY is unavoidable. Additionally, we observe that the contact angles become heterogeneous when the transition from nemato-philic to nemato-phobic occurs as shown in Fig. 3(b) and (g).

Experiments with the glass surfaces grafted with PEG strongly support the fact that the PEG molecules at the LCLC–glass interface are responsible for the wetting reversal. Utilizing silane chemistry, we graft PEGs to the surface of cleaned glass coverslips and use them as the confining wall for the sandwich cell, *i.e.*, LCLCs confined between two planar coverslips. Regardless of the length of PEG in mPEG-silanes ( $>5$  monomers), PEG-grafted surfaces become nemato-phobic as if PEG is added to bulk SSY. In other words, the nemato-phobic PEG-grafted glass inhibits the nucleation of the nematic phase and favors the isotropic phase when SSY enters the nematic–isotropic coexistence region from the isotropic phase. Note that even short PEGs can be effective when they are grafted to the glass surface,

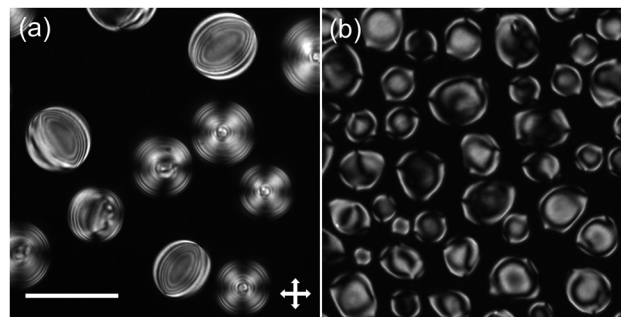


**Fig. 4** POM images of 30.0% (wt/wt) SSY entering the nematic–isotropic coexistence region from the isotropic phase at a temperature of  $55 \pm 2$   $^{\circ}\text{C}$ . The white double arrows represent the pass axes of crossed polarizers. The scale bar is 100  $\mu\text{m}$ . SSY in (a) is sandwiched between two glass slides grafted with mPEG-silane of 5-monomer PEG. SSY in (b) is sandwiched between two bare glass slides but doped with 0.1% (wt/wt) PEG of approximately 8 monomers, *i.e.*, molecular weight of 400. The nematic phase in (a) nucleates in bulk to form droplets of bipolar configurations while the nematic phase in (b) forms sessile droplets that partially wet the bare glass surfaces.

as shown in Fig. 4, while short PEGs added to the bulk do not change the wetting behavior probably because of low adsorption. Lastly, we mention that there is no observable change, *i.e.*, by  $\pm 1$   $^{\circ}\text{C}$ , in the nematic–isotropic transition temperature because of the PEG-grafted confining walls.

Adsorbed or grafted PEG molecules on the confining glass surfaces as crowding agents will induce condensation of the nematic phase in bulk, not on the surface. Otherwise, the nematic phase will wet the glass surfaces as shown in Fig. 2(a)–(c) and Fig. 4(b). We think that this mechanism takes place in the same vein with the well-known inhibition of non-specific binding and fouling by the steric shielding of hydrated PEG at the interface. We confirm the similar effects with PEG-derived surfactants, *i.e.*, Triton X-100 and Tween 60; the glass surfaces become nemato-phobic when the concentration of the doped surfactants is greater than  $\sim 5 \times 10^{-3}\%$  (wt/wt). These PEG-induced changes in wetting behaviors and molecular interactions involved need further study concerning the surface anchoring of LCLC.<sup>53</sup>

### Effects of PEG on the double-twist director configuration of the nematic phase

Here, we investigate how PEG doping affects the nematic director configuration of confined SSY. PEG-doped SSY in cylinders also shows the DT director configuration as in the case of neat SSY. The DT configurations of neat LCLCs in cylinders are well-characterized.<sup>11,12</sup> Fig. 1(e) shows the DT configuration  $\hat{\mathbf{n}} = -\sin\beta(r)\hat{\phi} + \cos\beta(r)\hat{\mathbf{z}}$  where the nematic directors have no radial component twist along the radius of the cylinder. Comparing Fig. 1(a)–(d) and Fig. 5(a), we find that the director configurations maintain the DT configuration, regardless of the existence of PEG dopants. Specifically, PEG-doped SSY also exhibits POM textures with parallel stripes and topological defects resulting from domains of different handednesses as shown in Fig. 1(c) and (f) and Fig. 5(a) and (d). However, note that PEG-doped SSY in square capillaries often

exhibits the parallel-axial configuration with no twist (see Fig. S2 in the ESI†) while neat SSY shows the DT configuration in the same square capillaries.<sup>57</sup>

We notice that PEG affects the DT configuration in two aspects: the emergence of a new defect and a heterogeneity in the director configuration. Firstly, in the DT configuration of PEG-doped nematic SSY, both domain-wall-like defects and point defects appear, as shown in Fig. 5(a), while the DT configuration of neat SSY exhibits only point defects<sup>11</sup> (see Fig. 1(a)). Note that a similar domain-wall-like defect has been reported in the DT configuration of nematic disodium cromoglycate,<sup>12</sup> but not in nematic SSY. It is reported that SSY's point defect shown in Fig. 1(f) has lower energy than the domain-wall-like defect shown in Fig. 5(d)<sup>11</sup> (see ESI† for a further discussion about the energy difference). Secondly, as shown in Fig. 1(a) and 5(a), the POM textures of the PEG-doped DT configuration not only look dissimilar to the textures of the neat one, in terms of the overall brightness and intensity ratios among the bright stripes, but also become heterogeneous within the same sample and even in the same domain. For instance, the far-left and far-right domains in Fig. 5(a) look different while the

two domains in Fig. 1(a) look identical (see Fig. S4 in the ESI† for additional data for comparison).

We propose that PEG addition may facilitate the formation of meta-stable director configurations. This explanation is first supported by heterogeneity in the observed POM textures. Because the POM texture is an indicator of how the directors twist in the DT configuration, *i.e.*,  $\beta(r)$  in Fig. 1(e), multiple POM textures imply that the configurations of different  $\beta(r)$  coexist in the sample. Different profiles of transmitted light intensities shown in Fig. 5(c) support this scenario. Note that  $\beta(r)$  is directly reflected in the transmittance through the central region of the capillary, *i.e.*, along the cylindrical diameter, as a function of angle between the crossed polarizers. This heterogeneity persists after a heating-and-cooling sequence, *i.e.*, melting into the isotropic phase and cooling back to the nematic phase, and after a long relaxation in the nematic phase over 24 hours. Additionally, we fail to get consistent number ratios among multiple POM textures and between the point defects and domain-wall-like defects, after analyzing five different capillaries having  $\approx 12.5$  cm length and  $\approx 300$  defects in total. The ratios change considerably in every heating-and-cooling trial; for instance, the ratios of point to domain-wall-like defect range from 5:5 to 3:7, although they might not be statistically significant because of the small number of defects investigated. Equilibrium director configurations would give a consistent number ratio according to the Boltzmann factor  $\exp(-\Delta E/k_B T)$  where  $\Delta E$  is the energy difference between two types of director configuration or defect. We believe that these observations indicate the kinetic nature of the formation of the director configuration.

We speculate that a PEG-induced change in the wetting behavior of the nematic phase on confining walls may contribute to the formation of the kinetically trapped director configurations. As shown in Fig. 2, PEG completely changes how the nematic domains appear and merge while the isotropic phase makes a transition into the nematic phase during the temperature decrease. In the PEG-free case, the nematic film on the capillary surface breaks up by the Plateau-Rayleigh instability to form cylindrical nematic domains separated by isotropic droplets (see Movie S1 in the ESI†). The cylindrical nematic domains relax to have the DT configuration of energy-minimizing  $\beta(r)$  with randomly assigned handedness as they grow and isotropic droplets shrink.<sup>8</sup> When an isotropic droplet between two hetero-chiral nematic domains disappears, a point defect forms as shown in Fig. 1(a)–(c) and (f). However, with the addition of PEG, the spherical nematic droplets, as shown in Fig. 2(f), grow and merge to form nematic domains. The nematic droplets of the bipolar configuration are randomly oriented, and thus their merging and defect formation look more disordered than the neat case, which seems to hamper the relaxation of the directors to the DT configuration and the well-known point defect (see Movie S1 in the ESI†). Note that this resembles the defect formation by the Kibble mechanism.<sup>58,59</sup>

We conclude our discussion by mentioning other considerations regarding the effects of PEG on the director configuration. First, PEG can change the elastic moduli of nematic SSY including twist, bend, and saddle-splay elastic moduli that participate in

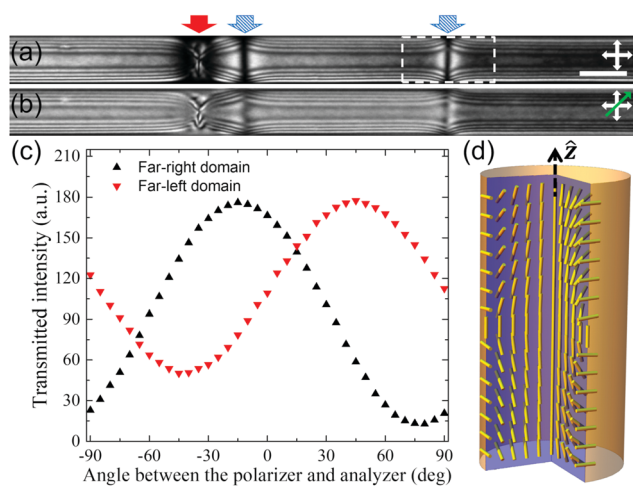


**Fig. 5** Topological defects and profiles of transmitted light intensities of PEG-doped 30.0% (wt/wt) nematic SSY in capillary tubes. The concentration of 35k PEG added is 0.01% (wt/wt). (a and b) POM images of the DT configuration of PEG-doped nematic SSY between crossed polarizers (a) without and (b) with a full-wave plate (550 nm retardation) under a quasi-monochromatic illumination at a wavelength of 660 nm. White double arrows represent the pass axes of the linear polarizers, and a green single-headed arrow indicates the slow axis of the full-wave plate. Note that, in (a and b) there are four domains separated by three defects including one point defect (pointed by a red-filled arrow) and two other domain-wall-like defects (pointed by blue-striped arrows), which have not been observed in the case of neat SSY, as shown in Fig. 1(a). Scale bar: 50  $\mu\text{m}$ . (c) Transmittance through the central region of the cylinder as a function of angle between the polarizer and the analyzer. The filled symbols (black and red) are experimentally measured transmittance from the far-right and far-left domains of (a), respectively. The standard deviation of the intensity from the central region, *i.e.*, a rectangle spanning up to 10% of the cylinder diameter, is smaller than the height of the symbols. (d) The suggested schematic diagram of the domain-wall-like defect highlighted by a dashed box in (a) based on a report by Davidson *et al.*<sup>11</sup> The yellow rods represent the nematic directors.

the DT configuration. Indeed, some additives such as salts affect the elastic moduli considerably despite their low concentration,<sup>46</sup> although the effects of neutral additives have not been reported, to our knowledge. Considering that the elastic constants determine not only the twist angle profile  $\beta(r)$ , as shown in Fig. 1(e), but also the type of defects between domains of different handedness,<sup>11</sup> this scenario of the changed elastic moduli may explain the emergence of the not-before-seen domain-wall-like defect. We look forward to the experimental determination of the elastic constants of PEG-doped SSY in the near future.<sup>2,4,46</sup>

The degenerate planar anchoring might not be valid with the adsorption of PEG molecules. Note that the whole argument regarding the DT configuration is based on degenerate planar anchoring.<sup>11,12</sup> If the anchoring changes by adsorbed PEG, *e.g.*, becoming non-planar with some polar anchoring angle, the DT configuration of  $\beta(r)$  and the defect must be reconsidered. For example,  $\hat{n}$  might have a radial component, and this can change the POM textures. Additionally, we cannot exclude possibilities that the PEG-adsorbed surfaces might acquire some anisotropy and inhomogeneity of the surface anchoring. The anisotropy or inhomogeneity can hinder the nematic LC from relaxing to a uniform DT configuration. We indeed observe the heterogeneity in the director configuration, *i.e.*, dissimilar textures within the same capillary, as manifested in the comparison of the far-left and far-right domains in Fig. 5(a).

## Conclusions

We discover a doping-induced wetting reversal in the nematic-isotropic coexistence phase of confined LCLCs and investigate the effects of PEG doping on their nematic director configuration. Despite a minuscule amount of added PEG, it makes the glass confining wall nemato-phobic by adsorption, for which the amount is determined by the bulk concentration and the molecular weight. Experiments with PEG-grafted glass surfaces also support the role of PEG as a surface blocking agent. We also report that PEG affects the nematic director configuration. Specifically, PEG-doped nematic SSY in a cylindrical cavity exhibits the DT configuration as in the case of neat nematic SSY. However, PEG doping results in the emergence of domain-wall-like defects and different POM textures. We propose multiple scenarios on how the DT configuration is affected by PEG.

Further studies on the effect of doping would benefit both fundamental understanding and applications of the LCLCs. Although there have been a series of investigations about the effects of dopants on LCLCs, mostly regarding their phase behaviors, studies on how and why LCLCs' elastic and anchoring properties get affected by dopants are still lacking.<sup>2,4,53</sup> As proposed in this work, a minuscule amount of dopants, which hardly affect the phase diagram, may considerably change the properties of LCLCs, *e.g.*, elasticity and surface anchoring, and thus tune the properties on demand. Indeed, we demonstrate that the dopant can modify interactions between the nematic phase and confining wall and induce wetting reversal, by the

adsorption of the dopant molecules onto the surface. In a similar vein, it is reported that the surfactants may play a key role in the uniform and stable alignment of LCLCs, which is essential for the study and applications of LCLCs.<sup>53</sup> We believe that thorough investigations of these surface interactions can contribute to the better control of LCLCs' surface anchoring property and open up new possibilities for the application of their nematic-isotropic coexistence phase.<sup>60</sup>

## Conflicts of interest

There are no conflicts to declare.

## Acknowledgements

The authors gratefully acknowledge the financial support from the Korean National Research Foundation through NRF-2015R1A2A2A01007613 (the director configuration) and NRF-2018R1C1B6002811 (the wetting behavior). Works by V. Sunkara, Y.-K. Cho, and J. Jeong were also supported by IBS-R020-D1 funded by the Korean Government.

## References

- 1 J. Lydon, *Liq. Cryst.*, 2011, **38**, 1663–1681.
- 2 S. Zhou, A. Sokolov, O. D. Lavrentovich and I. S. Aranson, *Proc. Natl. Acad. Sci. U. S. A.*, 2014, **111**, 1265–1270.
- 3 A. Masters, *Liq. Cryst. Today*, 2016, **25**, 30–37.
- 4 S. Zhou, Y. A. Nastishin, M. M. Omelchenko, L. Tortora, V. G. Nazarenko, O. P. Boiko, T. Ostapenko, T. Hu, C. C. Almasan, S. N. Sprunt, J. T. Gleeson and O. D. Lavrentovich, *Phys. Rev. Lett.*, 2012, **109**, 037801.
- 5 S. Zhou, K. Neupane, Y. A. Nastishin, A. R. Baldwin, S. V. Shiyanovskii, O. D. Lavrentovich and S. Sprunt, *Soft Matter*, 2014, **10**, 6571–6581.
- 6 L. Tortora and O. D. Lavrentovich, *Proc. Natl. Acad. Sci. U. S. A.*, 2011, **108**, 5163–5168.
- 7 J. Jeong, Z. S. Davidson, P. J. Collings, T. C. Lubensky and A. G. Yodh, *Proc. Natl. Acad. Sci. U. S. A.*, 2014, **111**, 1742–1747.
- 8 J. Jeong, L. Kang, Z. S. Davidson, P. J. Collings, T. C. Lubensky and A. G. Yodh, *Proc. Natl. Acad. Sci. U. S. A.*, 2015, **112**, E1837–E1844.
- 9 J. Ignés-Mullol, G. Poy and P. Oswald, *Phys. Rev. Lett.*, 2016, **117**, 057801.
- 10 K. Nayani, J. Fu, R. Chang, J. O. Park and M. Srinivasarao, *Proc. Natl. Acad. Sci. U. S. A.*, 2017, **114**, 3826–3831.
- 11 Z. S. Davidson, L. Kang, J. Jeong, T. Still, P. J. Collings, T. C. Lubensky and A. G. Yodh, *Phys. Rev. E: Stat., Nonlinear, Soft Matter Phys.*, 2015, **91**, 1–5.
- 12 K. Nayani, R. Chang, J. Fu, P. W. Ellis, A. Fernandez-Nieves, J. O. Park and M. Srinivasarao, *Nat. Commun.*, 2015, **6**, 8067.
- 13 A. Javadi, J. Eun and J. Jeong, *Soft Matter*, 2018, **14**, 9005–9011.
- 14 P. C. Mushenheim, R. R. Trivedi, H. H. Tuson, D. B. Weibel and N. L. Abbott, *Soft Matter*, 2014, **10**, 88–95.

- 15 P. C. Mushenheim, J. S. Pendery, D. B. Weibel, S. E. Spagnolie and N. L. Abbott, *Proc. Natl. Acad. Sci. U. S. A.*, 2016, **113**, 5564–5569.
- 16 D. Goldfarb, M. E. Moseley, M. M. Labes and Z. Luz, *Mol. Cryst. Liq. Cryst.*, 1982, **89**, 119–135.
- 17 H. Lee and M. M. Labes, *Mol. Cryst. Liq. Cryst.*, 1982, **84**, 137–157.
- 18 H. Lee and M. M. Labes, *Mol. Cryst. Liq. Cryst.*, 1984, **108**, 125–132.
- 19 M. Lavrentovich, T. Sergan and J. Kelly, *Liq. Cryst.*, 2003, **30**, 851–859.
- 20 M. Lavrentovich, T. Sergan and J. Kelly, *Mol. Cryst. Liq. Cryst.*, 2004, **409**, 21–28.
- 21 C. K. McGinn, L. I. Laderman, N. Zimmermann, H.-S. Kitzerow and P. J. Collings, *Phys. Rev. E: Stat., Nonlinear, Soft Matter Phys.*, 2013, **88**, 062513.
- 22 S. Yang, B. Wang, D. Cui, D. Kerwood, S. Wilkens, J. Han and Y.-Y. Luk, *J. Phys. Chem. B*, 2013, **117**, 7133–7143.
- 23 C. Peng and O. D. Lavrentovich, *Soft Matter*, 2015, **11**, 7257–7263.
- 24 F. Berride, E. Troche-Pesqueira, G. Feio, E. J. Cabrita, T. Sierra, A. Navarro-Vázquez and M. M. Cid, *Soft Matter*, 2017, **13**, 6810–6815.
- 25 T. Ogolla, S. B. Nashed and P. J. Collings, *Liq. Cryst.*, 2017, **44**, 1–11.
- 26 L. Bergquist and T. Hegmann, *ChemNanoMat*, 2017, **3**, 863–868.
- 27 T. Shirai, M. Shuai, K. Nakamura, A. Yamaguchi, Y. Naka, T. Sasaki, N. A. Clark and K. V. Le, *Soft Matter*, 2018, **14**, 1511–1516.
- 28 L. J. Yu and A. Saupe, *Mol. Cryst. Liq. Cryst.*, 1982, **80**, 129–134.
- 29 D. Perahia, D. Goldfarb and Z. Luz, *Mol. Cryst. Liq. Cryst.*, 1984, **108**, 107–123.
- 30 T. K. Attwood, J. E. Lydon, C. Hall and G. J. T. Tiddy, *Liq. Cryst.*, 1990, **7**, 657–668.
- 31 D. J. Edwards, A. P. Ormerod, G. J. T. Tiddy, A. A. Jaber and A. Mahendrasingham, *Physico-Chemical Principles of Color Chemistry*, Springer Netherlands, Dordrecht, 1996, pp. 83–106.
- 32 B. Neumann, *J. Phys. Chem. B*, 2001, **105**, 8268–8274.
- 33 H. von Berlepsch and C. Böttcher, *J. Phys. Chem. B*, 2002, **106**, 3146–3150.
- 34 L. Spindler, I. Drevenšek-Olenik, M. Čopič, J. Cerar, J. Škerjanc and P. Mariani, *Eur. Phys. J. E: Soft Matter Biol. Phys.*, 2004, **13**, 27–33.
- 35 A. F. Kostko, B. H. Cipriano, O. A. Pinchuk, L. Ziserman, M. A. Anisimov, D. Danino and S. R. Raghavan, *J. Phys. Chem. B*, 2005, **109**, 19126–19133.
- 36 S. K. Prasad, G. G. Nair, G. Hegde and Y. Jayalakshmi, *J. Phys. Chem. B*, 2007, **111**, 9741–9746.
- 37 O. Boiko, R. Vasyuta, O. Semenyshyn, Y. Nastishin and V. Nazarenko, *Ukr. J. Phys. Opt.*, 2008, **9**, 236.
- 38 H.-S. Park, S.-W. Kang, L. Tortora, Y. Nastishin, D. Finotello, S. Kumar and O. D. Lavrentovich, *J. Phys. Chem. B*, 2008, **112**, 16307–16319.
- 39 L. Wu, J. Lal, K. A. Simon, E. A. Burton and Y.-Y. Luk, *J. Am. Chem. Soc.*, 2009, **131**, 7430–7443.
- 40 J. W. Jones, L. Lue, A. P. Ormerod and G. J. T. Tiddy, *Liq. Cryst.*, 2010, **37**, 711–722.
- 41 L. Tortora, H. S. Park, S. W. Kang, V. Savaryn, S. H. Hong, K. Kaznatcheev, D. Finotello, S. Sprunt, S. Kumar and O. D. Lavrentovich, *Soft Matter*, 2010, **6**, 4157–4167.
- 42 J. P. De Almeida Martins, F. V. Chávez and P. J. Sebastião, *Magn. Reson. Chem.*, 2014, **52**, 540–545.
- 43 A. Alfutimie, A. P. Ormerod, D. J. Edwards, G. J. T. Tiddy, H. Wheatcroft and J. W. Jones, *Liq. Cryst.*, 2015, **42**, 1519–1526.
- 44 A. P. Ormerod, J. W. Jones, H. Wheatcroft, A. Alfutimie and G. J. Tiddy, *Liq. Cryst.*, 2015, **42**, 772–782.
- 45 B. Zhang and H.-S. Kitzerow, *J. Phys. Chem. B*, 2016, **120**, 3250–3256.
- 46 S. Zhou, *Lytotropic Chromonic Liquid Crystals*, Springer International Publishing, Cham, 2017.
- 47 A. Yamaguchi, G. P. Smith, Y. Yi, C. Xu, S. Biffi, F. Serra, T. Bellini, C. Zhu and N. A. Clark, *Phys. Rev. E*, 2016, **93**, 012704.
- 48 H. S. Park, S. W. Kang, L. Tortora, S. Kumar and O. D. Lavrentovich, *Langmuir*, 2011, **27**, 4164–4175.
- 49 K. A. Simon, P. Sejwal, R. B. Gerech and Y.-Y. Luk, *Langmuir*, 2007, **23**, 1453–1458.
- 50 J. G. Theis, G. P. Smith, Y. Yi, D. M. Walba and N. A. Clark, *Phys. Rev. E*, 2018, **98**, 042701.
- 51 D. Matsunaga, T. Tamaki, H. Akiyama and K. Ichimura, *Adv. Mater.*, 2002, **14**, 1477–1480.
- 52 C. Ruslim, D. Matsunaga, M. Hashimoto, T. Tamaki and K. Ichimura, *Langmuir*, 2003, **19**, 3686–3691.
- 53 P. van der Asdonk, P. J. Collings and P. H. J. Kouwer, *Adv. Funct. Mater.*, 2017, 1701209.
- 54 P. J. Collings, P. van der Asdonk, A. Martinez, L. Tortora and P. H. Kouwer, *Liq. Cryst.*, 2017, **44**, 1165–1172.
- 55 V. R. Horowitz, L. A. Janowitz, A. L. Modic, P. A. Heiney and P. J. Collings, *Phys. Rev. E: Stat., Nonlinear, Soft Matter Phys.*, 2005, **72**, 1–10.
- 56 R. L. Parfitt and D. J. Greenland, *Clay Miner.*, 1970, **8**, 305–315.
- 57 J. Fu, K. Nayani, J. O. Park and M. Srinivasarao, *NPG Asia Mater.*, 2017, **9**, e393.
- 58 M. J. Bowick, L. Chandar, E. A. Schiff and A. M. Srivastava, *Science*, 1994, **263**, 943–945.
- 59 Y.-K. Kim, S. V. Shiyanoskii and O. D. Lavrentovich, *J. Phys.: Condens. Matter*, 2013, **25**, 404202.
- 60 S.-D. Kim, B. Lee, S.-W. Kang and J.-K. Song, *Nat. Commun.*, 2015, **6**, 7936.